Nuclear Based MRI

SBE311 Medical Equipment II

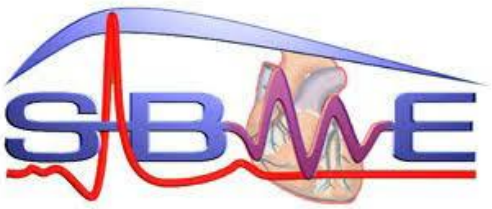

Under Supervision of:

Dr. Inas Yassin

TEAM NAMES:

MARWA ABDULLAH

SEC: 2, BN: 28, SEAT NO. : 53073

MENNATULLAH HAMDY

SEC: 2, BN: 35, SEAT NO. :53080

MOSTAFA YEHIA

SEC: 2, BN: 33, SEAT NO. :52078

FADY TADROUS

SEC: 2, BN: 13, SEAT NO. :53058

Table of Contents:

List of Figures:

List of Tables:

List of Abbreviations:

UTE:	Ultrashort Echo Time
ZET:	Zero Echo Time
NMR:	Nuclear Magnetic Resonance
PET:	Positron Emission Tomography
CT:	Computer/Computed Tomography
T_R:	Repetition Time
T_E:	Echo Time
T_1:	Recovery Time
T_2:	Relaxation Time
TOF:	Time of Flight
ZHBO:	Zero Helium Boil Off

Abstract

Positron Emission Tomography/Magnetic Resonance Imaging PET/MRI combines metabolic and molecular information of PET with excellent anatomic details of MRI systems to enhance the image quality. PET/MRI is applied for cancer in areas of the brain, neck, and pelvis, which require a good distinction between diseased and healthy tissue due to their complex anatomic structure. The usage of PET/MRI, especially in an integrated system, depends on the development of components that avoid deleterious interactions caused by high magnetic fields of the MRI scanner and RF interference between the MRI and PET systems.

Introduction:

The main difference between nuclear imaging and other radiologic tests is that nuclear imaging assesses how organs function, whereas other imaging methods assess anatomy, or how the organs look. The advantage of assessing the function of an organ is that it helps physicians make a diagnosis and plan present or future treatments for the part of the body being evaluated. Fast improvements in engineering and computing technologies have made it possible to acquire high-resolution multidimensional nuclear images of complex organs to analyze structural and functional information of human physiology for computer-assisted diagnosis, treatment evaluation, and intervention. Technological inventions and developments have created new possibilities and breakthroughs in nuclear medical diagnostics. The classic example is the discovery of Anger, fifty six years ago. The application and commercial success of new nuclear imaging methods depends mainly on three primary factors: sensitivity, specificity and cost effectiveness. The first two determine the added clinical value, in comparison with existing medical imaging methods. Nowadays, much greater importance is attached to cost effectiveness than in the past. This also holds true for diagnostic equipment where, for example, one of the consequences is that price erosion will occur where the functionality of an instrument is not open to further development. A PET/MRI system can help to improve diagnoses and to monitor treatments due to the combination of information and the resulting image enhancement of both systems. It provides intricate structural details compared to CT scans, especially in imaging soft tissues. If the PET system is fully integrated in an MRI system, examination times can be shorter because there is no need to move patients from one system to the other. Compared to PET/CT, the radiation dose is lower in PET/ MRI. Disadvantages from the view of the operators are the relatively high costs of PET/MRI systems. Recent Developments and Current Research Recent developments have integrated PET/MRI into clinical settings. In 2010, Philips introduced a system of a 3 T MRI system and a high-resolution PET scanner with an integrated rotating table, which allows sequential image acquisition by moving the patient from one machine to the other. The first integrated PET/MRI scanner was introduced by Siemens in 2011, which is able to do simultaneous whole body MRI and PET scans.

Sequence objective

MRI generates multiple soft tissue contrasts through the use of different pulse sequences. These pulse sequences define how the MRI scanner excites hydrogen atoms in water molecules to create signals and how spatial information is encoded using magnetic field gradients. Excitation of hydrogen atoms, also commonly referred to as “spins,” is performed with radio-frequency (RF) fields, which are created by RF transmit antennas, commonly referred to as “coils.” RF receive antennas/coils are used to receive the signal coming from spins after excitation. Magnetic field gradients, referred to as “gradients,” change the magnetic field at different spatial positions, which allow for encoding of spatial information. Gradients can be applied in the X, Y and Z directions (G_X, G_Y and G_Z), which allow for creation of images in arbitrary scan planes (axial, coronal, sagittal, and any oblique orientation). Gradients are also used for encoding motion information such as flow and diffusion [15].

As the signal intensity in standard MRI sequences is dependent on combinations of proton density and tissue relaxation, all hybrid PET/MRI systems are mainly affected by suboptimal attenuation correction factors for emission results, not directly related to the electron density and linear tissue attenuation coefficients as in PET/CT. So it is not straightforward to use MRI metrics for

attenuation correction and many methods have been attempted to perform an effective segmentation of MRI data according to tissue class [1].

A transmission scan is used to produce an attenuation map that is co-registered to the T1-weighted MRI images. The MR image is eventually segmented into areas with different attenuation values (bone, brain tissue, fluid, and air in the paranasal sinuses), and this attenuation map is then applied to the PET images [2].

Sequence description

A whole-body acquisition is included in the workflow for many PET/MRI studies; thus simultaneous whole-body MRI protocols need to optimize overall scan efficiency. Many entire-body MRI techniques have been developed that can be applied to PET/MRI. Whole-body diffusion-weighted imaging is especially challenging, workflows often aim for 3 – 5 min per bed position to keep a reasonable overall scan time [3]. Pulse sequences that are inherently fast by design are typically used in PET/MRI protocols. These include single-shot fast spin echo (SSFSE) for T_2-weighted imaging [4] and two-point Dixon [5] for T_1-weighted imaging. Single-shot fast spin-echo pulse sequences acquire a complete 2D image following a single RF excitation. Due to T_2 decay during the long train of refocusing RF pulses and high levels of energy deposition to the patient, the main limitations of this technique are blurring, respectively counterbalanced by relatively low resolution and long repetition times.

Technical developments now adopted by all major vendors have improved speed and resolution[6], so that single-shot fast spin echo can now achieve adequate resolution and repetition times of less than a second per slice, which allows full coverage of motion-prone regions (chest, abdomen) in a single breath-hold. While the clinical acceptance of single-shot fast spin echo is increasing, conventional fast spin echo (FSE, TSE, RARE) is still often preferred for the generally superior image quality, despite the considerably longer acquisition times and associated motion sensitivity. In particular, STIR (short-tau inversion recovery) [7] and radial fast spin-echo imaging are commonly used. STIR is a fat- suppression preparation, whereby all spins are inverted before the RF excitation is played out and the start of the host pulse sequence is timed to coincide with the time when the longitudinal magnetization of fat is zero. While this ensures uniform fat suppression even in the presence of large field in homogeneities, which are often present given the large coverage required for whole-body imaging, SNR is significantly degraded as all the other tissues are also recovering according to T_1 at the time of excitation; therefore, longer scan times are generally necessary to achieve adequate signal levels. Radial fast spin echo is a fast spin-echo-based technique where the central part of k-space (the spatial frequency space where raw MR signals are stored before image reconstruction) is repeatedly sampled during the acquisition [8]. A dedicated image reconstruction exploits this data redundancy to create motion-free images during free breathing [9].

While image quality can be superior to single-shot fast spin echo (higher resolution, reduced blurring), motion insensitivity comes with longer acquisitions that can be problematic, especially in the context of whole-body imaging.T_1-weighted imaging is often performed using high-resolution 3D gradient-echo pulse sequences [10]. Water/fat resolved imaging, is often used for the excellent image quality, speed, and the characteristic of providing several image contrasts in a single acquisition, namely, a “water only” image (similar to a fat-suppressed image), an “in-phase” image (effectively a nonfat-suppressed image), an “out-of-phase” image characterized by a dark rim between water and fatty tissues, and a “fat-only” image that depicts only fat- containing tissues (Figure 1). While water-/fat-separated imaging can often achieve relatively high-image resolution, depending on the specific implementation, there can be a limit on the maximum matrix size that the user can prescribe. In these cases, other fat-suppression methods (SPECIAL, SPAIR) can be used in conjunction with conventional fast 3D gradient-echo pulse sequences for high-resolution, fat-suppressed T_1-weighted imaging.

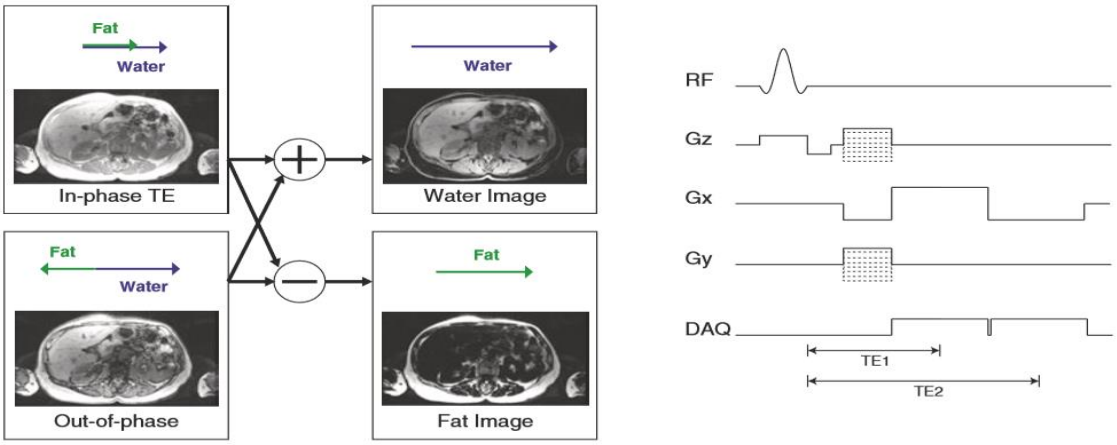

Figure 1: Fat/water imaging using a two-echo Dixon acquisition

A recently proposed alternative for T1-weighted imaging, with excellent motion properties, is 3D radial gradient-echo imaging [11]. The MR signals are encoded according to a stack-of-stars pattern, whereby several "stars" are consecutively acquired to cover the desired 3D volume. Because the center of k-space is repeatedly sampled for each "star," motion artifacts can be greatly mitigated by advanced image reconstruction algorithms. In general, considerations on speed, as well as robustness to motion and system imperfections (B0 and B1 in homogeneities), often dictate which pulse sequence should be used for a specific protocol. Accelerated imaging strategies such as parallel imaging and compressed sensing can be used to speed up the acquisition, at the cost of reduced signal-to-noise ratio and with performance dependent on the specific array coil used for signal reception. Parallel imaging methods are standard on clinical PET/MRI systems, under the names ASSET and ARC (GE) and mSENSE and GRAPPA (Siemens). These methods use receive coil arrays, under sample data in k-space, and use specialized image reconstructions. Compressed sensing utilizes the inherent sparsity of MR images to accelerate acquisitions [12], which is now implemented for some pulse sequences in current commercial scanners. The use of compressed sensing will likely increase in the future [15].

1. MR Attenuation Correction:

Accurate PET reconstruction requires an estimate of the photon attenuation prior to detection. In the body, there is a range of attenuation in soft tissues, and bone attenuation is higher than soft tissues. In PET/CT systems, the attenuation is derived from CT, which is a direct measurement of the electron density that determines the attenuation. However, MRI measures signals from protons, and does not provide any direct measurements of electron density.

This has proven to be a challenge for PET/MRI, and current promising strategies are based on imaging atlases as well as specialized pulse sequences for soft tissue and bone imaging [15].

2. Fat/Water Imaging:

Many MRAC strategies use fat-water separation imaging methods, also known as "Dixon" or "IDEAL" methods [5]. These methods acquire data at multiple echo times (TEs). Since fat and water have different resonance frequencies due to their chemical shift, they will appear with different phases as a function of TE. With the known frequency shift between fat and water, images of the fat fractional signal and water fractional signal are generated with these methods. These can then be used to account for the differences in attenuation between fatty tissues and water soft tissues.

The principle of fat/water imaging methods is illustrated in Figure 1. In an ideal situation, images are acquired at two different TEs, chosen such that fat and water are "in phase" for one TE and "out of phase" for the other. These images then can be used to generate fat and water images. In reality, the phase also evolves as a function of TE due to resonance frequency shifts due to magnetic field in homogeneities. This can be accounted for by either acquiring a third TE image to explicitly measure these field variations or by using only two TE images with some assumption of spatial smoothness of the field variations .For MRAC, typically two-point Dixon approaches are used, as they are faster and the smooth field variation assumption has been shown to be robust for clinical imaging.

The RF body coil is typically used for transmit and receive, as local receive RF coil arrays can introduce undesirable variations across the images. To provide the volumetric coverage required, 3D gradient-recalled echo (GRE) sequences with two TEs are used as shown in Figure 1. The two TE images are then combined to generate fat-fraction and water-fraction images from which soft tissue attenuation coefficients can be assigned [13][15].

3. Bone Imaging:

Conventional MR imaging pulse sequences do not detect any signal from the bone due to its rapid MR signal decay rate (T2* ≈ 0.4 ms). This has been a major challenge in PET/MRI because the bone has the largest photon attenuation among all tissue types but is difficult to image with MRI. Neglecting the bone leads to large errors in PET uptake in and around the bone, measured to be between 10% and 15% [14]. Specialized MRI pulse sequences, so-called ultrashort echo-time (UTE) and zero echo time (ZTE) pulse sequences, offer the potential to capture the rapidly decaying signal from the bone and thus are being actively developed and applied to improve MRAC.

Conventional MRI pulse sequences, such as the gradient-echo sequence illustrated in Figure 1 have minimum TEs of approximately 1 ms. this is due to the time required to play out a slice-selective RF pulse as well as the frequency and phase- encoding gradients. UTE and ZTE can achieve TEs below 100 μs on clinical MRI scanners by using specialized RF pulse and image-encoding strategies, examples of which are shown in the pulse sequences in Figure 2. For RF excitation, the TE can be minimized by using volumetric excitation with no slice-selection, minimum- phase slab excitation (UTE only), or half-pulse slice-selective excitation (UTE only). For image encoding, radial k-space sampling is most commonly used (as shown in Figure 2), but spiral or cones k-space trajectories are also possible [16] (UTE only).

These encoding strategies require using a non-uniform Fourier transform reconstruction. ZTE also has the unique property of near-silent scanning but requires advanced reconstructions or additional acquisitions to fill in missing data at the center of k-space. Due to its low proton density and rapid decay rate, bone has a relatively low signal even with UTE and ZTE MRI. This signal difference has been used to estimate bone density for attenuation correction from ZTE MRI. MRAC including the bone has also been accomplished by separating the bone based on its relaxation rate, T2* [30 – 35]. Fat/water separation can be included in UTE MRI by adding additional TEs and using the processing methods described in the previous section [15].

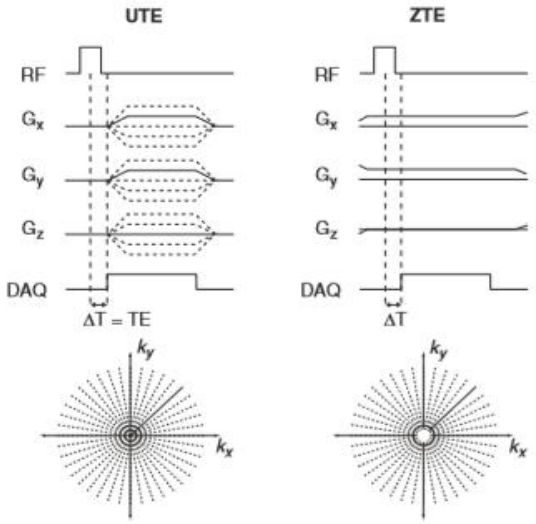

Figure 2: UTE and ZTE MRI pulse sequences that can image bone for estimation of tissue attenuation coefficients

4. Diffusion-Weighted Imaging:

Water molecules diffuse in biological tissues under the effect of Brownian thermal motions. Because the diffusion of water molecules is restricted by the presence of obstacles, such as macromolecules, membranes, etc., measuring the diffusivity of these molecules in different tissues provides information on the underlying microstructure. The more cellular the tissue, the more restricted the diffusion. Diffusion-

weighted imaging (DWI) is often achieved by playing out two identical gradient lobes on either sides of the refocusing RF pulse of a spin-echo pulse sequence. Immediately after the RF excitation pulse, all spins are aligned along the same direction in the transverse plane. While the first gradient lobe is played out, static spins diphase at a rate that depends on the local magnetic field imposed by the gradient itself.

The refocusing RF pulse flips them over, while the direction of dephasing remains unchanged. Because these spins are static, they experience exactly the same local magnetic field while the second gradient lobe is applied, so that at the time of the spin echo, they end up back in phase as if no gradients were played out. Diffusing spins, unlike static spins, experience slightly different local magnetic fields before and after the refocusing RF pulse, as their spatial location in the direction of the applied gradients has slightly changed due to random motion at molecular level. As a result, at the time of the spin echo, not all spins end up back in phase, and the measured signal is reduced by a factor that depends on the mean diffusivity of water molecules in that specific tissue. Similar to T2-weighted imaging, where longer TEs are used to increase the amount of T2 weighting, larger diffusion-sensitizing gradients can be used to increase the amount of diffusion weighting. In practice, the amount of diffusion weighting is expressed by a quantity called b value. The higher the b value, the higher the amount of diffusion weighting. A standard T2-weighted image is also a b=0 image (i.e., no diffusion-sensitizing gradients applied).

A heavily diffusion- weighted image will be characterized by low signal intensities in regions of unrestricted diffusion (fluids) and high signal intensities in areas of restricted diffusion (e.g., tumors). In truth, high signal intensity in a diffusion-weighted image can be due to either restricted diffusion or long T2. Apparent diffusion coefficients (ADC) can be computed from two diffusion-weighted images with different b values to provide a measure of diffusivity independent of T2. From an acquisition point of view, diffusion-weighted imaging typically relies on echo-planar imaging (EPI), because of its speed, signal-to-noise efficiency, and robustness to motion. However, EPI is also extremely sensitive to off- resonance, leading to significant distortion and image artifacts, especially for whole-body imaging [15].

5. Whole-Body Diffusion-Weighted Imaging

Distortion is proportional to the local off-resonance field and the duration of the EPI readout. Whole-body imaging requires large anatomical coverage, which means relatively long readouts even for a modest image resolution. At the same time, field in homogeneities due to eddy currents, susceptibility variations, chemical shift, and other system imperfections are more difficult to control over large imaging volumes. Parallel imaging techniques are routinely used to reduce distortion, although their effectiveness is limited by the performance of the specific coil array used for signal reception.

Higher-order eddy current compensation strategies, either prospective or retrospective, are often implemented to reduce distortion induced by eddy currents. STIR is the preferred fat-suppression method for whole-body imaging due to its robustness to B0 and B1 in homogeneities, despite the lower intrinsic SNR. Chemically selective fat-suppression methods (fat pre-saturation, spectral-spatial RF pulses, and gradient reversal), even when used in combination, can result in fat-suppression failures that translate in chemical shifts of several pixels across the imaged FOV. Signal averaging during free breathing is routinely used to compensate for the otherwise low SNR due to STIR, and usually no more than two b values are acquired to avoid lengthy acquisitions. Free-breathing diffusion- weighted imaging using STIR and signal averaging is referred to as DWIBS (diffusion- weighted imaging with background suppression). Whole-body diffusion imaging is typically performed axially, with coronal/sagittal reformats generated for the purpose of visualization.

A common artifact observed in sagittal reformats is the typical stair-step appearance of the spine, due to center frequency mismatch between different beds. Recently developed prospective and retrospective corrections aimed at minimizing this artifact have greatly improved the appearance of sagittal and coronal reformats of whole-body imaging datasets [15].

6. Lung Imaging:

A significant limitation to widespread clinical implementation of PET/MRI is poor evaluation of the lung parenchyma. Pulmonary imaging is challenging for MRI due to low tissue density, motion, and rapid signal decay rates with $T2^* \approx 0.5 – 3$ ms [17]. With these limitations, MRI detection rates of large pulmonary nodules (>1 cm) are high; however, the detection rate of sub centimeter nodules remains inadequate for routine clinical evaluation.

The ultrashort echo-time (UTE) and zero echo-time (ZTE) MRI pulse sequences, described previously for bone imaging to improve MRAC (Figure 2), are also a promising approach for lung imaging. They can capture the rapidly decaying signals in the lung and additionally are much more robust to motion than conventional pulse sequences.

3D imaging is typically used (similar pulse sequences to Figure 2), though often with slab-selective excitation to minimize aliasing artifacts [18]. To compensate for motion and improve image quality, randomized ordering strategies and self-gating from the repeated central k-space sampling can be applied. Compressed sensing and parallel imaging strategies can also be incorporated to improve image quality [15].

7. Workflow: General Strategies

PET/MRI protocols all share some common aspects. First, MRI localizers have to be acquired (corresponding to the scout scan or topo gram in PET/CT) to plan the subsequent acquisition and define the axial range for the joint PET/MRI examination. Next, the number and localization of bed positions of the PET acquisition have to be defined using the localizer. PET usually works in the so-called step-and-shoot mode, in which the two main acquisition parameters to be defined are the number of bed positions and the acquisition time for each bed position.

In the scanners currently used, the axial range of a single bed position is about 25 cm, with a certain percentage of overlap between adjacent bed positions (depending on the vendor). The acquisition time can either be kept similar to that in PET/CT, typically 2–4 min per bed position, or this time can be increased to make use of the potentially longer time required for the simultaneous MRI sequences. Similar to PET/CT, the PET data can either be acquired in a dynamic way as list-mode data or as a static acquisition. In principle, it is also feasible to acquire PET and MRI data while the patient bed is continuously moving, as recently described for combined PET/MRI [19].

This extremely interesting approach might substantially facilitate the workflow for whole-body PET/MRI but is not yet routinely integrated in currently used PET/MRI systems. The major technical advantage is the reduction in sensitivity “drop” at the edges of the field of view, which should in theory also result in a more flexible acquisition time. However, also an improvement concerning psychological burdens has been described. Claustrophobic patients seem to appreciate the continuous motion as it actually suggests an ongoing procedure instead of “waiting” for the next bed position. The time needed for the PET acquisition can then be used to acquire the needed MRI data for each bed position. There is only one mandatory MRI sequence, which is the one used for attenuation correction (AC) as the attenuation data in PET/MRI are derived from the MRI scan [20].

This sequence is usually acquired first for each bed position. There are various techniques used for AC in PET/MRI, but most commonly a two-point or three-point Dixon sequence is used. A separate breath-hold acquisition is necessary for each bed position, which usually takes about 14–19 s per bed position for higher-resolution T_1 imaging. This sequence is preceded by scanning preparations that include shimming to optimize the homogeneity of the magnetic field. The MRI data are then segmented to identify air, lung tissue, fatty tissue, and watery tissue as required for AC [21].

The Dixon sequence has been found valuable for anatomic localization of PET-positive lesions, as the sequence is acquired over the whole field of view (i.e., all PET bed positions) and can be nearly isotropic [22]. Other approaches in use for MRI-based AC are using a three- dimensional T_1-weighted sequence as in the sequential PET/MRI scanner [23]. However, one major disadvantage of these techniques is that the bone is neglected, which might be of special relevance in areas with a high density of the bone like the skull or the pelvis. To partly compensate for that problem, one vendor is currently using a CT atlas for the attenuation correction of the head. One potential, more general solution to this problem is the use of an ultrashort echo time/zero echo time sequence to identify bone, like used routinely in one system for the skull and brain imaging [24]. Moreover, other atlas-based techniques can be used for identification of the bones [25]. There are also now different region-specific solutions being developed [26], as well as there are intentions to use zero echo time imaging for whole body attenuation correction.

After acquisition of the data for AC, the MRI component can be used to acquire any further sequences within the current field of view, simultaneously with the corresponding PET acquisition, which runs in parallel. Currently there are no restrictions in the choice of MRI sequences in hybrid PET/MRI scanners. The MRI sequences can also extend beyond the PET acquisition time planned for the current bed position, with the rest of the examination being consequently delayed.

Image Contrast in MRI

There are 3 parameters (intrinsic features of biological tissue) that are responsible for constructing image and its intensity or brightness which are: … [27]

1. Proton Density
2. T_1 Time
3. T_2 Time

Proton Density

Definition:

Number of excitable spins per unit volume, determines the max signal obtained from a given tissue

Contrast-Image:

Images are called *proton density weighted* or *proton density images*

Control:

- Minimizing the other two parameters (T_1 and T_2)

T_1 Time

Definition:

The time tissue takes for the excited spins to recover and be available for the next excitation, affects intensity indirectly

Contrast-Image:

Images are called *T_1 weighted images (T1W)*

Control:

- Can be varied at random
- Increase/Decrease External Magnetic Field B_0

T_2 Time

Definition:

The time which determines how quickly an MR signal fades after excitation

Contrast-Image:

Images are called *T_2 weighted images (T2W)*

Control:

- Controlled by the operator
- Increase/Decrease External Magnetic Field B_0

Repetition Time (T_R) and T_1 Weighting

Repetition Time (T_R)

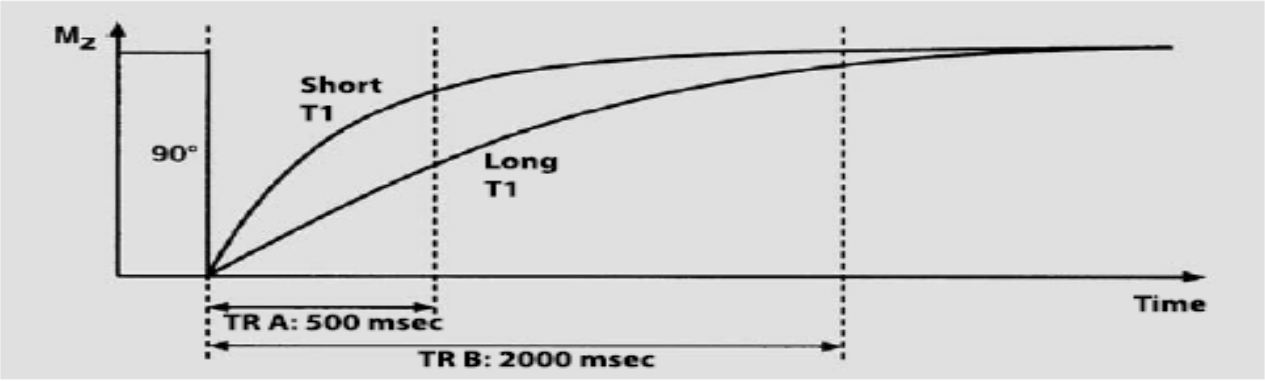

Figure 3 Relation between T_R and T_1

The interval between two successive excitations of the same slice

Short T_R means strong T_1 Weighting.

Long T_R means low T_1 Weighting.

Tissue with short T_1 appear ***bright*** because they regain most of their longitudinal magnetization during T_R, producing ***stronger*** MR signal.

Tissue with long T_1 appear ***dark*** because they don't regain much of their longitudinal magnetization during T_R, producing ***weaker*** MR signal.

Echo Time (T_E) and T_2 Weighting

Echo Time (T_E)

The interval between applications of the excitation pulse and collection of MR signal
Short T_E means low T_2 Weighting.

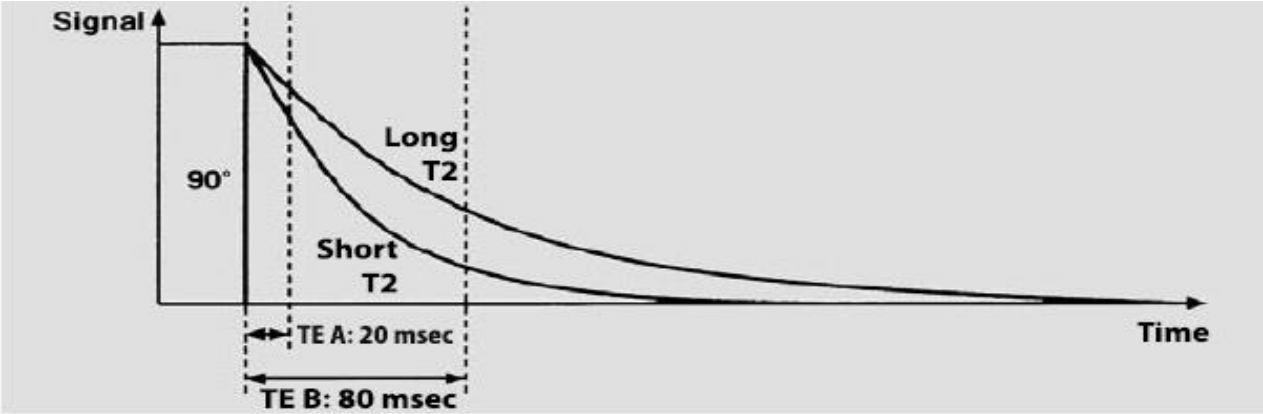

Figure 4 Relation between T_E and T_2

Long T_E means strong T_2 Weighting.
Tissues with a short T_2 appear ***dark*** on T_2 weighted images,
Tissues with a long T_2 appear ***bright*** on T_2 weighted images.

Following table (Table1) summarize relations between T_R and T_E: … [27]

	T_R	T_E
T_1-WEIGHTED	Short	Short
T_2-WEIGHTED	Long	Long
PROTON DENSITY WEIGHTED	Long	Short

Table1. Summarize relation between the parameters of MRI

Flip Angle (Tip Angle)

Flip angle can be used to minimize saturation and get enough MR signal even if there is a short T_R.

Image Contrast in PET scan

There is no technique uses only a PET scan nowadays, it's a combination between PET and CT or PET and MRI and we will illustrate why by the following sections. First to be established was PET/CT scan and it had its own features and advantage which turned into disadvantages/limitations later on so that we moved to PET/MRI technique which had a lot of advantages and less dangerous … [28][15].

PET/CT scan

It may be impossible to accurately localize an area of increased activity on PET images alone due to absence of identifiable anatomic structures (e.g. Abdomen). Then prototype PET/CT scanner used in clinical imaging, at which we can determine coregistered functional and anatomic images by performing PET scan and CT scan on the same scanner without moving the patient … [28].

PET/MRI scan

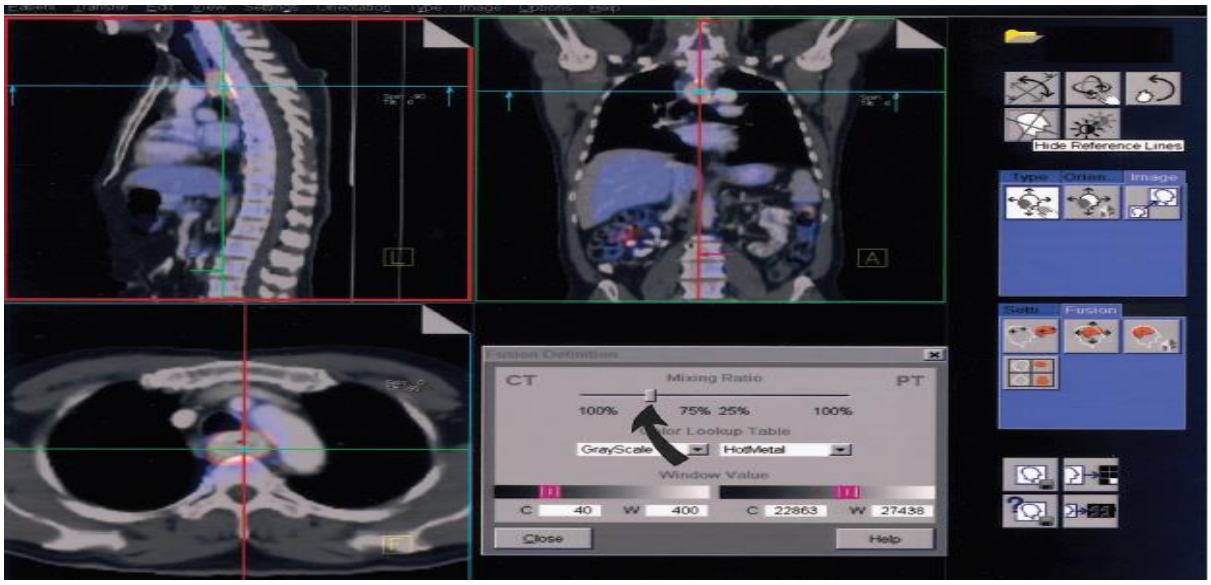

Figure 5 Display of PET/CT image using an application called syngo

PET/MR not only provides soft tissue contrast and minimizes pro-radiation, but also a wealth of MR properties such as functional and spectroscopic imaging, the combination of PET/MR has proven to be a major challenge due to the effects of scanners on each other's performance … [29]

There were many issues that were limiting the possibility of mixing the PET with the MRI and it must be known well without going into its details in this part. These issues are known by compatibility issues and they are (static magnetic field, magnetic susceptibility, eddy currents, coil loading, temperature, mechanical vibration, interference and gamma attenuation).

What matters in the PET / MRI device is its design as it is based on the following elements (photodetectors, radiofrequency shielding, data transmission, gamma shielding, hardware attenuation and cooling). The following figure shows and explains the old type PET/MRI system.

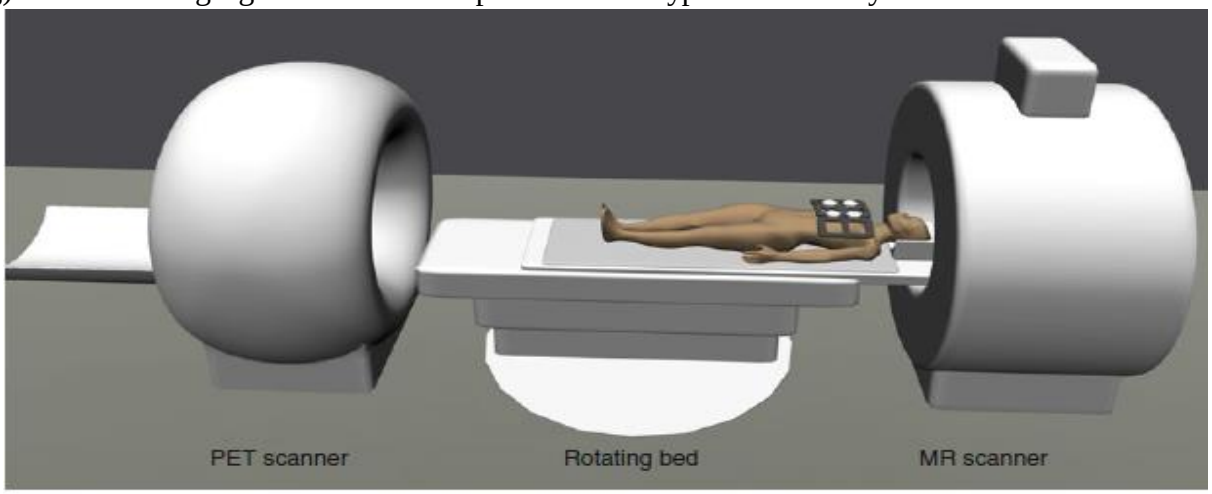

Figure 6. PET/MR system

As for the current PET/MRI devices, there is no agreement entirely on its complete picture or the nature of its original shape, but there is no doubt that its business idea is the basic thing agreed upon in all of this. We will have a look on Siemens' machine that combines both PET and MRI scans.

PET/MRI Instrument

Historically, there were not any instrument that apply both techniques together (PET and MRI) scanners. So, what was done is the following. MRI scan is firstly done on patient to generate image about selected area then patient is moved to PET scan directly using movable bed to detect if there is a problem in blood flow, tumor failure … etc. But this is not the perfect way to do such a scan on a patient taking into

consideration the magnetic field applied in MRI machine and its risks and also the radioactive tracer in PET machine and its risks.

Currently, many medical companies are seeking to develop a PET/MRI scan in a single machine. Siemens did that already in machine called (Biograph mMR) which we will go further in its details, components and way of work.

So why we change from PET/CT to PET/MRI, let's see … (Further Details) [29]

Limitations of PET/CT scan

1. Low soft tissue/tissue contrast in important organs (e.g. Brain, Breast, Heart, Liver, Kidney and Bone)
2. Mis-registration artifacts due to motion
3. Gated CT to improve PET alignment and quantification is associated with relatively high radiation dose
4. Although the limit of resolution of PET scan alone compared to PET/CT scan remains approximately the same, the combination between them aids in the accurate localization of regions of increased activity on PET images with greater confidence.

Advantages of PET/MRI scan

1. Improved lesion detection (e.g. Brain, Liver, Bones, Kidney)
2. Improved delineation of tumor margins
3. Reduced radiation exposure (Specially "young adults")
4. Evaluation of other diseases such as cancer in patients

Advantages of simultaneous PET/MRI scan

Measuring multiple parameters simultaneously with optimal quantitative accuracy and lesion alignment

Manufacturers … (Wikipedia) [15]

1. Clinical systems

The first two clinical whole-body PET/MRI systems were installed by Philips, in 2010. The system featured a PET and MRI scanner separated by a revolving bed. Siemens was the first company to offer simultaneous PET/MR acquisitions, with the first systems based on avalanche photodiode detectors. In 2013, Apollo Hospitals launched the first PET/MRI in South Asia.

Currently Siemens and GE are the only companies to offer a fully integrated whole body and simultaneous acquisition PET/MRI system. The Siemens system (Biograph mMR) received a CE mark and FDA approval for customer purchase in 2011.

The GE system (SIGNA PET/MR) received its 510K & CE mark in 2014.

2. Preclinical systems

Currently, the combination of PET and MRI as a hybrid imaging modality is receiving great attention not only in its emerging clinical applications but also in the preclinical field. Several designs based on several different types of PET detector technology have been developed in recent years.

Several companies offer MR-compatible preclinical PET scanner inserts for use in the bore of an existing MRI, enabling simultaneous PET/MR image acquisition.

Now let's talk about biograph mMR developed by Siemens Company, it's the machine to involve both PET and MRI scans in a single machine.

Biograph mMR

This machine as we mentioned before combines between PET scan and MRI scan in it, its specifications, technique and defiantly shape is all what we are about to illustrate in the this section. First of all, the shape and design of biograph mMR came after many studies and researches and reached its final shape as shown … (Link1) (Link2)

Figure 7. Biograph mMR Siemens Company

Biograph mMR works by the principle of ZHBO which is the complete supply of helium gas. Its performance is dependent on helium's cooling. Helium is extracted from natural gas, which makes its availability very limited. If helium reaches the atmosphere, it will escape to space and will be lost forever.

Now we will talk about some benefits for environment due to this machine, operating data and technical specification in the net section.

Environmental Benefits

1. Better Energy
2. No Transportation
3. Dealing with 3T Magnetic Field
4. ZHBO

Operating Data

Heat Emission

Basic Load: <= 27 KW

Full Load: 33 KW

Room Temperature

18 ℃ - 22 ℃

Room Humidity

40 – 60 %

Power-on Time

15 min

Technical Specifications

1. Interface for heat recovery
2. Water Cooling
3. No complete switch-off

MR image Reconstruction

As a regrettable consequence of the considerable redesign effort needed to make PET compliant with the strong magnetic field produced by the MRI system, none of the PET / MRI systems currently available are equipped with a CT detector. This forced manufacturers to find alternative ways to create an attenuation map, based on available data from PET and MR.

The image contrast in magnetic resonance imaging, however, is based on the relaxation patterns of hydrogen nuclei, which are related to proton density and tissue chemistry. These reflect completely different physical principles than those involved in photon scattering / attenuation which are related to tissue elements' interactions with the electron shell. Consequently, a simple, continuous mapping of MRI measures to attenuation values cannot be obtained, as was the case with PET / CT [30]. Instead, attenuation correction based on MRI (MRAC) involves more sophisticated approaches, mostly depending on a priori knowledge of the imaged object [31].

1. Segmentation-Based MRAC

All three clinical PET/MRI systems manufacturers have opted for a segmentation-based approach to their simple attenuation correction method [32]. The idea behind segmentation-based MRAC is to acquire a predefined MRI sequence and then apply a series of post-processing steps to partition the image into a given set of tissue classes. Then each voxel image is assigned an a priori attenuation coefficient according to the class of tissue to which it belongs (e.g. air, lung, fat, and soft tissue).

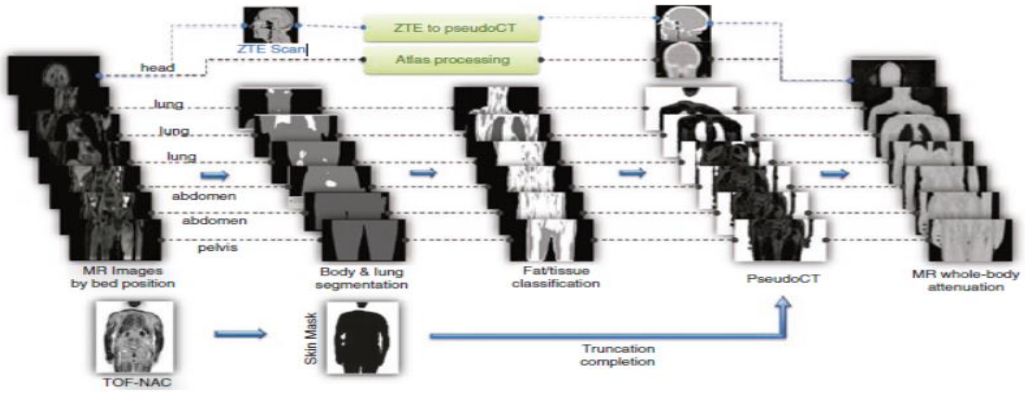

Figure 8. Example of MRI-based attenuation correction, as implemented in the SIGNA PET/MR

The number of tissue classes considered is perhaps the most critical parameter of those methods. The Ingenuity TF uses a three-class model (air, lung, and soft tissue) for whole-body imaging, whereas the Biograph mMR and SIGNA PET / MR use a four-class model (air, lung, fat, and soft tissue) that enables voxels to provide intermediate values between fat and soft tissue classes [33].

Keereman et al. concluded that at least five classes (air, lung, soft tissue, spongy bone and cortical bone) should be considered for improved precision, with the addition of a sixth class (adipose tissue). With this setup, PET errors below 5 % are reported. Ouyang et al. report 4%, 7%, 13%, and 15% (for fat, soft tissue, bone, and lung respectively) errors when using a four-class model. They also conclude that a three-class model is sufficient when imaging the heart, liver, or kidneys to obtain errors below 5 %.

The specific values assigned to those classes are almost as significant as the number of classes of tissues considered. For the lung the Ingenuity TF uses 0.0219 cm-1; for the lung the Biograph mMR assigns 0.0240 cm-1; for the lung the SIGNA 0.0180 cm-1. A point of agreement between the two above-mentioned studies is, in particular, the desirability of considering the inter-patient variation of lung tissue, something not yet applied in any of the commercial systems [34].

Usually fast T_1-weighted acquisitions are the preferred MRI sequences for tissue segmentation purposes, short enough to be acquired in a single breath-hold (~20 s per bed position). In the case of the Ingenuity TF a simple sequence of gradient-echo with body coil receives suffices. On the other hand, the Biograph mMR and SIGNA PET / MR require double-echo sequences capable of fat/water differentiation: a coronal Dixon-VIBE with local coil receives for the Biograph, and an axial LAVA-FLEX with body coil receives for the SIGNA [35].

It should be remembered that the dual-echo processing used for these sequences is susceptible to a certain form of artifact called "fat/water swap". Restricted to the edge of the field of view where the decreased homogeneity of the magnetic field is causing the misclassification of small regions. However, in some exceptional cases (e.g. patients with large fluid accumulations) this was known to cause large portions of the attenuation map to be misclassified.

The receive coil used to obtain the MRI signal is also a important factor. In terms of SNR surface coils positioned directly on (or below) the patient provide the best image quality, as well as enabling acceleration through parallel imaging. On the other hand, the built-in body coil provides more homogeneity in strength, leading to a more stable post-processing of the images. This involves a trade-off between the possibility of obtaining diagnostic-quality MRAC images (saving the time of a second T_1-weighted acquisition) and giving users greater freedom in their patient setup.

2. Bone Attenuation

Most of the clinical PET/MRI devices currently available involve the bone in its default attenuation correction based on segmentation. The explanation for this is the difficulty of regular MRI sequences to visualize the bone. Nevertheless, bone tissue is characterized by a low proton density (it only contains 20 percent water) and a heterogeneous structure that induces rapid dephasing of MRI signals (T2 ~ 390 μs at 3 T) [36].

On the other hand, there has been frequent coverage of the value of accounting for bone attenuation Ignoring bone attenuation is known to induce both quantitative and qualitative bias in the brain (within the range (−20%, −10%)) and in the vicinity of large bone structures in the body.

Of this reason, some manufacturers have alternative methods of attenuation correction of regions like the head and hips. To this end, two key approaches exist: the recording of anatomical atlas details on the default MRAC images and the acquisition of short echo time sequences capable of capturing the rapidly decaying signal from the bone [37].

The SIGNA PET / MR contains a head station atlas based method. It relies on the no rigid registration, based on CT data, of a pre-recorded head atlas to the same LAVA-FLEX acquisition used by the default MRAC. This approach has the advantage of not requiring additional acquisition time and being very robust to image artifacts (e.g. caused by metallic implants), apart from the incorporation of bone information [38]. In the minus side, isomorphic differences of patient anatomy can only be accounted for. In other words, the registration can't build holes: a patient with a craniotomy will result in a full skull attenuation map; a toothless patient will result in a map with teeth attenuating. Likewise, the approach does not compensate for inter-patient density variation, since the model determines the attenuation coefficients (e.g., pediatric patients may have a separate atlas because of their substantially different bone tissue density). Likewise, the approach does not compensate for inter-patient density variation, since the model determines the attenuation coefficients (e.g., pediatric patients may have a separate atlas because of their substantially different bone tissue density) [39]. None of these developments, however, have made it into clinical practice yet. A bone MRAC system based on the ultrashort echo time (UTE) series [40] is used in the Biograph mMR. UTE is a radial acquisition with a tweaked, fast excitation pulse that enables sub-millisecond echo times, capable of capturing some of the short-lived bone tissue signal. T2 * values can be estimated by performing a dual-echo acquisition and used to identify the bone. In other words, by comparing the images from the first and second echoes, voxels can be identified and labeled as bone with a especially rapid signal decay.

Recently a similar method was released for the SIGNA, in this case using a sequence of zero echo time (ZTE) [36]. ZTE is also a radial center-out acquisition, with the peculiarity that the fields of gradients are not ramped down between excitations. This imposes some limitations on the sequence (e.g., nonselective excitation) but enables even shorter echo times, increasing the signal obtained from the bone. This can be exploited to perform single-echo acquisitions for bone segmentation, with the corresponding savings in scan time.

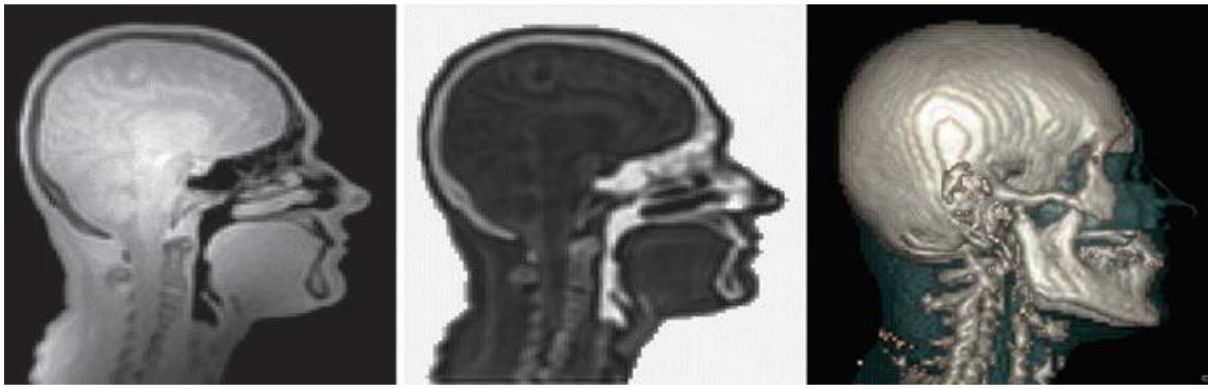

Figure 9. ZTE Example

In the literature several possible improvements have been reported for these methods. They include modifications to the sequences to increase the acquisition speed, in combination with Dixon fat / water separation methods and more elaborate post-processing to reduce the number of unwanted structures classified as bone [40].

Unfortunately, it is difficult to apply these techniques to other anatomical regions other than the head (e.g., greater FOV, cardiorespiratory and peristaltic motion, variable coil configuration, etc.). Recently a promising new atlas-based approach for the hip and thigh region was introduced, focusing on individual registration of a collection of bone components (femur, pelvic parts, and spine) [41].

3. Truncation Correction

The field of view can be a problem too in the attenuation correction of MRI or even CT when it's smaller than the scanner bore. When this happens, certain elements (usually the arms and shoulders of the patient) may fall outside the field of view, resulting in an incomplete map of the attenuation. If left uncorrected, this leads to artifacts, proportional to the sum of uncounted attenuation, in the restored PET images. The artifacts will typically be maximum on the truncated regions and will rapidly decline away from them, with a pattern that depends on the algorithm for reconstruction [42].

In PET/MRI the problem is more difficult to manage than in PET/CT, first of all, the typical MRI field of view is significantly smaller than that of CT (between 40 and 45 cm, compared to the 50 cm of CT). Indeed, the FOV's trans-axial scale is not constant as in CT but narrower at each station's axial core and smaller at the margins. More importantly, due to the projective nature of the acquisition CT data still contain data about the truncated regions. This can be used to create reconstructions which are corrected by truncation [43]. In contrast, truncated regions cannot be recovered from MRI data, and the missing attenuation information must be obtained from alternative sources.

Siemens reported a method for enabling MRI acquisition beyond the usual field of view by applying an optimized read gradient to compensate for static field inhomogeneity and gradient field nonlinearities limiting the range of regular sequences [44]. The main disadvantages of this approach are the relatively long acquisition time and the need for different gradients of readings — and hence separate acquisitions — on each patient side.

The PET measurements themselves provide yet another readily accessible source of knowledge about the truncated areas. Indeed, the default truncation correction strategies applied in clinical PET/MRI systems rely either on the segmentation of non-attenuation-corrected PET reconstructions or on the calculation of raw emission data attenuation information.

3.1 PET Segmentation

The idea behind the segmentation method is simple: define the patient body in the recovered emission images, and use that information to fill in the attenuation map's truncated regions (the PET field of view typically encompasses the whole scanner bore). The fairly easy concept has several caveats:

First, it means that the radiopharmaceutical is causing ample unspecific absorption to differentiate the patient body from the context. Although this can usually be accurate for most PET health conditions, it can become a severe restriction with more sophisticated tracers.

Second, while emission images can outline the patient, they contain little information about the different classes of tissue involved. Accordingly, truncation correction approaches based on segmentation usually assign a constant attenuation value to the recovered regions.

Finally, note that correction of the truncation is a necessary step in correction of the attenuation, which in effect is a necessary step in reconstruction of PET. It follows that non-attenuation-corrected (NAC) images of emissions used for truncation correction must be those. Unfortunately, on standard NAC images, the patient's contour is badly distorted (e.g., concavities are lost). However, in the case of Time-of - Flight (TOF) systems, NAC images show the correct patient contour due to the increased robustness of the TOF reconstruction to inconsistent data [45].

3.2 Joint Estimation of Emission and Transmission

Many researchers have tried to jointly estimate the operation picture and emission data attenuation to reduce the need for additional transmission calculation. These attempts were not very successful for SPECT and non-TOF PET, although Mihlin and Levin have recently published promising results for non-TOF PET at very high iteration numbers. This method was never used in clinical practice, except in situations where the issue could be managed due to the availability of much prior knowledge. However, the implementation of time of flight clearly improves the PET results, resulting in reconstructions with increased SNR and enhanced robustness against results incoherence.

Salomon et al. restricted joint estimation algorithm with contours obtained from the MRI image and achieved excellent results for the Philips TOF-PET/MRI system. Soon after, it was shown that TOF-PET data are indeed sufficiently rich to enable a stable joint reconstruction of the attenuation factors and the activity image up to a single scale factor, provided the activity is spread over an object that is large compared to the TOF resolution. It has been shown that the correct behavior and attenuation images can be reconstructed with a joint estimation method for 18F-FDG, which has a significant uptake almost anywhere in the body. There are several ways to estimate the attenuation by using TOF. The straight way is to measure the image of the attenuation.

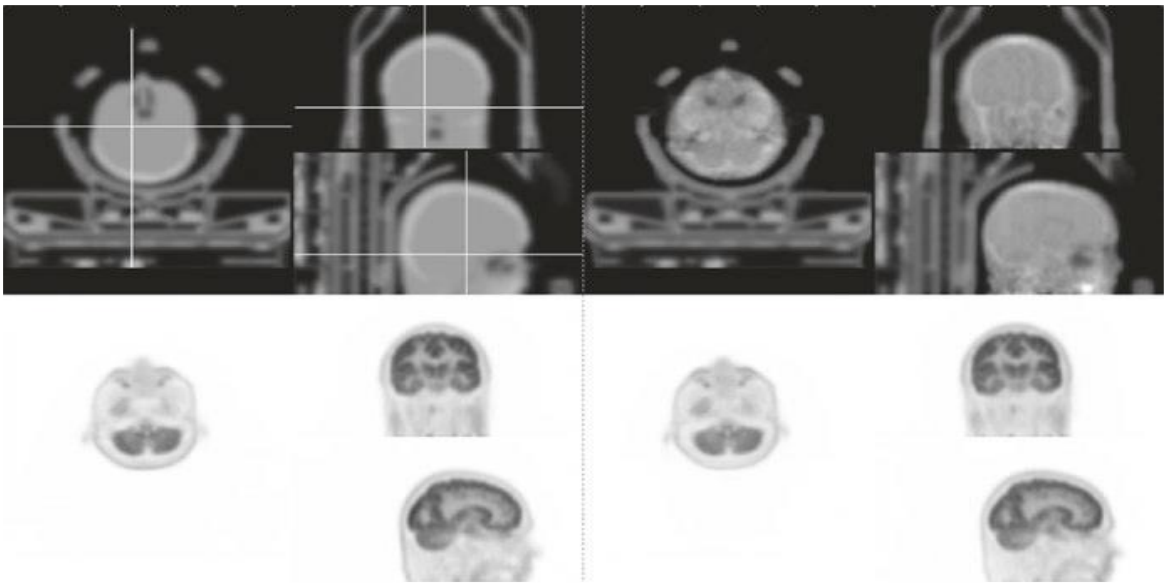

Figure 10. Left: The approximate attenuation on the GE SIGNA PET / MR device for a brain scan. Hardware attenuation is derived from a template; an atlas based approach estimates the attenuation of the patient's head. Right: The patient's head attenuation was calculated in conjunction with the MLAA algorithm [72] and the same hardware design. Images of the related attenuation-corrected operation are also shown.

This method is demonstrated in the last figure, where the TOF-PET data attenuation estimate is contrasted with the MRI-based attenuation plot. Alternatively, the TOF information can be used to estimate the sinogram attenuation (i.e., the sinogram with the attenuation factor for each response line (LOR)), without specifically specifying that this sinogram corresponds to the forward projection of the attenuation picture. I Where a potentially inconsistent attenuation image is available (as would usually be the case with PET/CT), the TOF information can be used to estimate a (no rigid) deformation that optimally aligns this attenuation image with emission data. As the number of TOF-capable hybrid PET / MRI systems is growing, joint estimation is an important approach to improving attenuation correction in MRI.

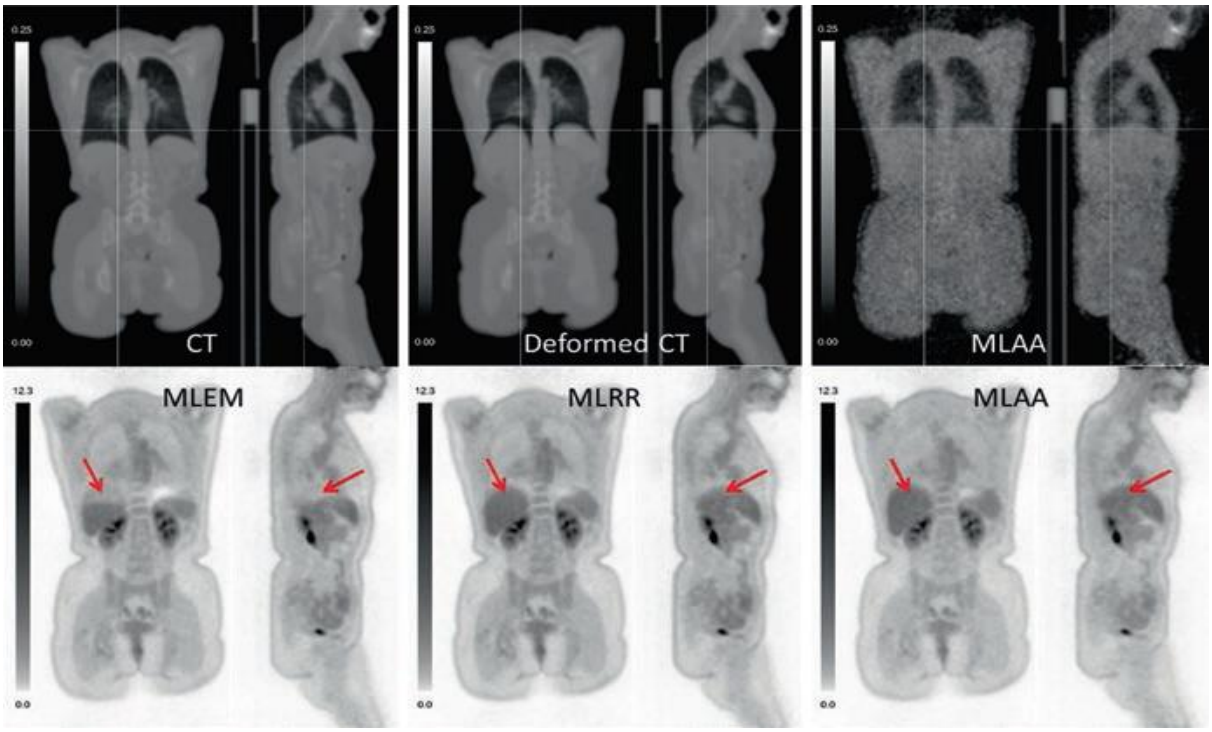

Figure 11. The CT-based attenuation and attenuation-corrected operation on the Siemens mCT for an entire body scan. Part of the liver is under-corrected for attenuation because the CT was taken during inhalation (left). The MLRR algorithm deforms the CT to optimize the TOF-PET data's probability, accounting for the mismatch (center). The consequence of MLAA is shown in column three.

This estimation of reciprocal attenuation and action is not without problems. One is that some prior knowledge is needed to estimate the scale factor: multiply the activity picture with a constant, and divide the attenuation sinogram into the same attenuated sinogram with the same constant result. Note that a scaled attenuation sonogram does not correspond to a scaled attenuation image; the scale factor expresses itself in the attenuation image as a place-based change in intensity. If the attenuation is measured as an image of the attenuation coefficients, this image can be segmented (partially) to define a soft tissue region and change the scale factor to reconstruct this area with the defined attenuation coefficient at 511 keV (0.00875 / mm for fat and around 0.0099 / mm for other tissues). If the attenuation is determined by deformation of an available attenuation map, the attenuation map will automatically evaluate the scale factor. If the attenuation is calculated as a sonogram of attenuation factors, then unfortunately it is not straightforward to evaluate the scale factor.

Another problem is that some LORs provide very limited information on attenuation, particularly those on which the activity is concentrated in the image processing of a small region (relative to the TOF resolution), and those on which a few photon pairs are measured. Typically this is the case with LORs near the edge of the piece. As a result, the joint calculation is performing poorly near to the patient body boundary. This issue will be more pronounced for tracers which have a more focused accumulation than 18F-FDG. MRI or CT supplying anatomical details is very helpful here.

The validation of the algorithms for the common estimation is less straightforward than one would expect. An easy solution would be to use the MLEM reconstruction as the gold standard using a CT-based attenuation chart (after checking that there is no inconsistency due to patient motion). However, when there is some incoherence in the data, MLEM and the methods of joint estimation converge to different results. That is because MLEM can only use the activity values to "explain" the data contradictions, while the attenuation values can also be manipulated by the joint estimation process. These incoherencies may be caused by any imperfection in the model of acquisition. Scatter correction is very difficult, and although the current scatter estimation algorithms are efficient, the scatter estimate is still approximate and can often vary substantially from the true scatter contribution.

Given these issues, a promising approach to improving attenuation correction in PET/MRI is the joint estimation. The concurrently obtained MRI image provides an abundance of anatomical details that can be used to resolve the limitations of the joint estimate, while the joint estimate provides the attenuation coefficients that cannot be deduced from the MR image. Manufacturers are continuing to improve the TOF resolution of their devices, and joint estimate efficiency will increase accordingly. Existing methods may be combined to generate a system that imposes strong restrictions based on the MR image when correcting the image for a potential misalignment that defines the scale factor by enforcing the known attenuation on some of the structures found in the MR image and estimates the attenuation of the rest [15].

Unsolved Artifacts

There are still many remaining artifacts that haven't been solved yet. In some cases, like patient solution remains unavailable in other cases, such as MRI metal artifacts. We will talk about them motion, solutions are slowly being incorporated into commercial systems, while a practical and what is the latest progress in solving these problems.

1. **Metal Artifacts**

It's already known from PET / CT that metallic implants interfere with attenuation correction [46].In PET / MRI, however, the physical principles involved are completely different: metal artifacts in CT are caused by the loss of transmission information in response line that intersects a high-attenuation object. This results in the images with bright starlike structures, from which long streaks radiate (sometimes across the whole image). In contrast, in MRI, metal artifacts are caused by changes in static and gradient fields which are caused by the metallic object's magnetization. This results in approximately spherical regions larger (~1–5 + cm) devoid of signal.

Many metallic implants, including pacemakers and neurostimulators, are potentially counter-indicated for MRI imaging. However, many implants are commonly permitted in clinical PET / MRI, for which a solution would be desirable. This is especially relevant for indications such as oncology, which mainly involves elderly patients and where hip, shoulder and dental prostheses are frequently found [47].

If left uncorrected, signal-void regions of the sequences used for MRAC caused by metal implants will cause those regions to be classified as air in the attenuation map. It could contribute to bias in the reconstructed PET images, based on the location of the implant but also extending to the surrounding area. [48].

Several correction methods have been suggested in the literature, either by finding patient gaps and filling them with tissue attenuation or by image painting [49,50] or by using multi-spectral MRI sequences capable of recovering the signal around metal[51]. Unfortunately both of these approaches have functional disadvantages. For example, assuming large cavities are caused by artifacts and should be filled with tissue is a valid assumption for certain regions (and one used by some systems), such as the pelvis and legs. But applying this same assumption in the abdomen requires careful consideration to avoid classification errors of the bowel air. The signal-void regions are also often quite large and can connect to the background, making their detection and correction complicated.

Interestingly, recent results show that reconstruction of the time of flight has a mitigating effect on metal artifacts. This is due to Data Inconsistencies due to the increased robustness of TOF reconstruction. It is important to note, however, that TOF does not make these errors go away, simply distributing them differently (maybe more conveniently) in the field of view.

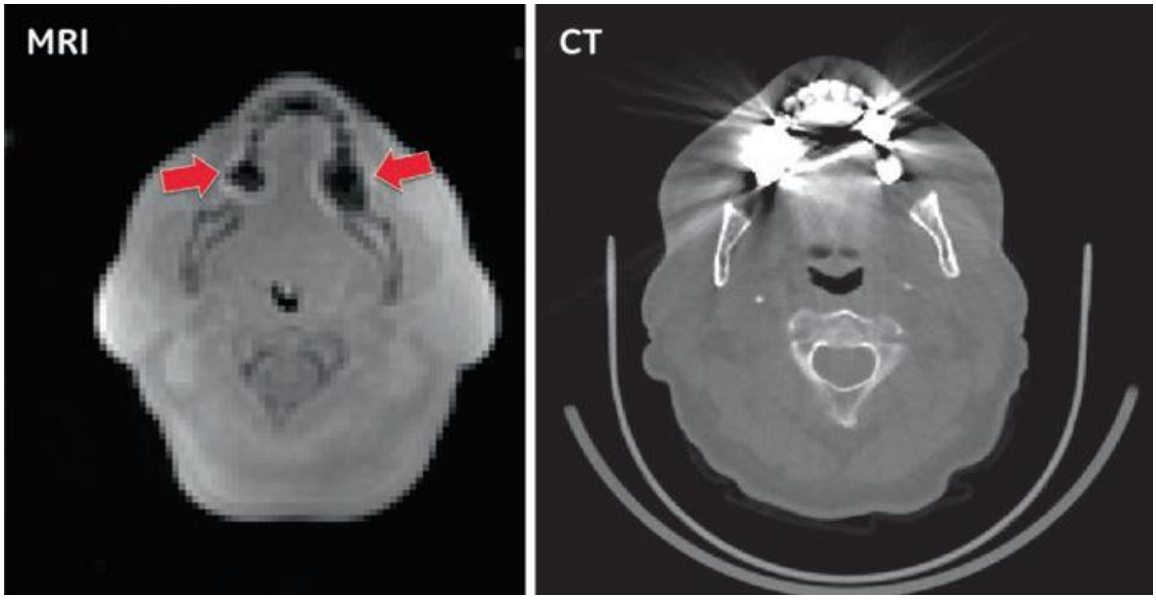

Figure 12: Axial views showing artifacts in MRI and CT caused by metallic implants

2. **Motion Artifacts**

Patient motion is a common source of artifacts in nearly every modality of imaging. Patient motion leads to a discrepancy between the attenuation map and the corresponding emission data for PET imaging, especially when considering attenuation correction. This results in taking bias around the moving regions, such as the well-known "banana artifacts" seen in PET / CT images around the diaphragm.

Patient motion problems include many distinct situations, such as periodic motion (e.g., cardiorespiratory), irregular motion (e.g., tremors), and bulk motion (e.g., repositioning). Despite the common underlying principles regarding the formation of artifacts, addressing these issues requires quite specific solutions, and they are best regarded as completely independent problems.

Maybe the best known and most widely researched case of cardiorespiratory motion. The PET / CT literature contains several potential solutions, usually relying on some kind of dynamic CT acquisition [52-15]. As a matter of fact, some consider PET / MRI's ability to provide radiation-free dynamic imaging as one of the main — unexploited — strengths of this modality. An increasing number of publications about correction of respiratory motion in PET/MRI can be found. However, the issue of attenuation correction is often lost during the acquisition of emission data as part of the bigger problem of compensating patient motion.

A crucial point to note is that while full-fledged motion correction is technologically complicated and not always simple for incorporation into clinical practice, motion-corrected attenuation correction is fairly easy to incorporate and administer. Indeed, the MR sequences used attenuation correction can be adjusted readily to produce four-dimensional data sets describing the respiratory cycle. Regular PET gating techniques can be used with these in hand to match the emission and attenuation datasets. As a side note, reconstruction of the time of flight has also been reported to reduce artifacts of respiratory mismatch.

Unlike respiratory motion, head motion is better suited for the implementation of motion correction (several manufacturers have introduced it in their products), and there is no benefit to addressing motion only on the attenuation map. By contrast, with head attenuation correction approaches now incorporating longer MRI sequences capable of bone imaging, movement during acquisition can have a noticeable effect on the attenuation map [53]. With marker-based or markerless optical motion tracking systems, head motion can be tracked with precision. Others are MRI compliant: Its use will avoid the loss of MR scanning time for motion tracking and provide high temporal resolution motion data to both devices , allowing motion correction [54].

3. **Contrast**

Relatively little research has been done on the effect of MRI contrast agents on attenuation correction based on the MRI. The actual attenuation of the sample is not affected by contrast agents but rather by the acquisitions of MRI used to estimate the attenuation map.

One concludes that bias attenuation maps are not expected to be associated with gadolinium-based T1 contrasts, while a more recent study reveals that these agents could potentially influence fat / water separation. Generally, contrast-enhanced sequences will be acquired after all acquisitions have been made for attenuation correction.

On the other hand, an iron oxide-based contrast T2 * was reported to potentially cause artifacts of susceptibility and maps of bias attenuation. In this case the additional drawback of some T2 * shortening preparations' long persistence time (weeks to months in uncommon cases) is present [55,56].

Precautions and preparations needed to be preformed

In order to improve radiation control in the test, because patient welfare is the most important consideration, the hospital or clinic manager shall create a committee on medical radiation safety management consisting of radiologists, radiation protection supervisors (if necessary by the Radiation Hazard Prevention Act), medical radiologists, pharmacists, nurses, etc. Periodically and whenever necessary, the manager shall hold a committee meeting to discuss the matters shown below. All decisions made at the meeting shall be issued to the appropriate departments in writing [57].

The medical radiology worker shall conduct a system acceptance test to confirm the normal operation and other functions of the system to be used for examinations after delivery to the examining facility and before use in actual examinations and confirm that it functions as described in the manufacturer's instruction manual with the attendance of the system distributor. In order to ensure their quality, the medical radiology worker must also periodically check system functions related to the approval criteria [57].

The medical radiology worker, etc., shall implement safety function monitoring and maintenance programs of the system used for inspection.

The quality assurance inspection must include an image acquisition time check, image acquisition method, and image processing method (image reconstitution method, filters, etc.). The performance of the computer system used for the acquisition and processing of images must be checked and test steps included [58].

If a significant system defect is discovered, the medical radiology worker, etc., shall notify the hospital or clinic manager of remedial measures taken temporarily, the manufacturer's subsequent repairs and the results of tests performed prior to restarting the system's clinical usage. In addition, the manager shall warn all medical radiology staff who run the program to these facts by announcing them publicly and telling them in writing [57].

Since FDG's "fluorodeoxyglucose" is the most common injection in PET, in the next discussion we will focus on that. In order to reduce radiation exposure in medical radiology workers involved in the preparation of FDG chemicals and/or PET examination and public exposure to radiation from patients undergoing PET examination as the source of radiation, the risk must be minimized to the lowest possible level within a fairly achievable range for medical radiology workers handling FDG chemicals, etc., and patients receiving them, by making the finest usage of the three principles of radiation safety (time, distance, shield), and taking into consideration social and economic factors [57].

PET radionuclides have short half-lives, and therefore they have to treat huge quantities of radioactivity releasing photons of high-energy annihilation. Therefore, the level of exposure in medical radiology workers is expected to rise during FDG production and dispensing, and FDG chemicals administration, etc. Radiation safety steps must be taken that are suitable to the characteristics of PET tracers. Because the exposure level depends on the time, the medical radiologist must be very skilled in the operating procedures during which radionuclides are managed and the distance from the source. For example, attempts must be made to shorten the period during which the worker is in interaction with the patient receiving PET chemicals, etc., providing patient instructions by approaching him or her at a distance greater than the minimum allowable level, by presenting details beforehand (i.e., an description of the nature and procedures of the test, the position of the examination room, and the means of moving from the waiting room). Before the FDG Review begins. In cases where urine excreted by the person undergoing FDG chemicals, etc., is pooled in the controlled area for a variety of medical reasons (pooled urine), it must be considered a radiation source on the day of FDG administration [57].

The contraindications and precautions for both modalities are accounted for by patient preparation for PET/MRI. Therefore, as for F-fluorodeoxyglucose PET in PET/CT, the criteria include a four-hour duration, blood glucose level control, and patient rest following FDG injection to reduce muscle uptake. PET/MRI contraindications are the same as for MRI, e.g., metallic implant and pacemaker checks, and for PET, e.g., pregnancy [58].

Patient placement for PET/MRI needs to be much more precise than needed for PET in order to maximize the MRI-image signal and avoid artifacts, specifically with respect to patient centering on the image couch and positioning of the surface coils. Positioning thus takes longer than it does for regular PET, and can potentially introduce radiation to workers. Therefore, workers should be qualified in both PET and MRI preferentially. Key topics to discuss with patients are:

1. Dietary restrictions to regulate blood stream amount prior to scan.
2. Recent injections of glucose or traumas which can disturb metabolic activity.
3. Aggressive activity.

Overall, there is a really little difference regarding patient safety/preparation between PET/MRI examinations versus PET/CT and MRI examinations [59].

Usefulness compared to other modalities

Combined positron emission tomography with magnetic resonance imaging (PET/ MRI) is a new promising technique that can replace PET/CT in selected cancer scenarios and can create new oncological uses. In PET/CT, CT compensates for the severely limited spatial resolution of PET, providing useful anatomical and morphological information complementary to PET's metabolic and molecular knowledge, making it a crucial investigation in the staging and re-staging of a wide range of cancers [57].

Some of the issues in PET/CT include the addition of the CT radiation dose and the limited CT soft-tissue contrast resolution. However, MRI not only offers superior contrast resolution between different soft tissue types, it also allows the observation of physiological (e.g., dynamic contrast enhanced MRI), metabolic (e.g., MR spectroscopy) and molecular (e.g., diffusion-weighted imaging) phenomena. Based on these advantages, hybrid PET/MRI scanners may be expected to have a superior PET/CT solution in some cancer imaging applications [58].

Soft tissue visualization is another essential aspect of in vivo imaging. MR is known to excel in evaluating various soft tissue structures with its range of different contrast weightings over CT capabilities. This is especially important in the field of small-animal imaging, where the use of contrast agents is often problematic. An example of PET/CT vs PET/MR imaging of small animals. An experiment was performed, a mouse was injected with a tracer [18F] fluoro-2-deoxy-D-glucose (FDG) to test the metabolism of glucose. The non-contrast enhanced CT reveals both the animal outline and the subcutaneous tumor just between. The bones alone demonstrate a superior contrast. Providing an equivalent CT contrast would require an injection of approximately 300 µL iodine-based contrast agent into a mouse with approximately 2.5 mL of blood volume. The resulting MR image shows an excellent soft tissue contrast that enables tumor tissue differentiation as well as abdominal organs (e.g., kidneys and spleen) to differ. It is obvious that MR can improve the accuracy of the diagnosis and allows a differentiation between the necrotic and vital tumor tissue, for example. Such data can then be compared to areas where the tumor has low and high tracer uptake. Studies showing that PET / CT is superior in lymph node screening as compared with whole body MR (wb-MR), while wb-MR is highly active in detecting distant metastasis. Not only does the field of oncology benefit from the soft tissue contrast that MR offers, neurology applications also need the anatomical and functional imaging capabilities of PET/MR [60].

Like in PET/CT, PET/MR allows a perfect co-registration of the PET and MR image data. This offers the possibility to use MR-derived anatomical landmarks to interpret the functional data obtained from the PET images. However, PET/CT co-registration has certain shortcomings especially in the abdomen and thorax due to the sequential nature of the data acquisition. Even dedicated breathing protocols in patient studies cannot avoid mis-registration between PET and CT. PET/MR machines can bypass this disadvantage with a simultaneous data acquisition. Therefore, movement artifacts are less pronounced by simultaneous PET/MR acquisitions [60].

This fascinating combination also offers no additional MR radiation dose, superior soft tissue contrast and a multitude of PET tracers, the combined PET/MR applications are profound in oncology and

require the imaging of the four key cancer formation processes: apoptosis resistance, angiogenesis, proliferation and metastasis. PET/MR also has many clinical and research applications that will be discussed later in neurology and cardiology. As regards their relevance to PET / MR, alternative techniques such as image fusion, hyperpolarized imaging and whole-body diffusion are discussed. Multifunctional and anatomical simultaneous imaging using PET/MR has tremendous potential for impacting biomedical imaging in research and clinics [60].

In addition, neuro-oncology and neuroscience are considered to be potential key applications for PET / MRI in clinical practice and research, since both modalities provide complementary morphological, functional, (patho)-physiological and molecular information about the human brain. The main advantage of integrated PET / MRI systems for neurology applications is seen in the data acquisition simultaneity, which allows both temporal and spatial cross-correlation and potential cross-validation of PET and MR measurements. Simultaneous PET/MRI would provide a better understanding of the functional (BOLD-fMRI), hemodynamic (arterial spin labeling (ASL), proton-weighted imaging (PWI), [^{15}O] H_2O PET) and metabolic (dynamic PET with various radiotracers, MR spectroscopy) interactions during brain stimulation as well as in various neurological disorders. In addition, the use of MRI data is thought to help improve PET quantification through, for example, motion correction. To balance these problems, correction of MR-based attenuation in the brain remains problematic especially around dense areas of the skull [61].

Dual time-point amyloid PET/MRI allows for an integrated approach to dementia imaging. More precisely, early post-injection amyloid imaging can be used as a measure of neuronal integrity, while delayed amyloid imaging contains information on amyloid charge in the brain; anatomical MRI investigates morphological changes such as atrophy, vascular lesions, and space-occupying lesions. Alternatively, MR-based ASL may be useful when acquired in parallel with the amyloid PET signal to provide information regarding neuronal injury [61].

Simultaneous PET/MRI also provides early evidence that changes in neurotransmission and neuronal activity and brain networks can be detected at the same time, which may help to improve the development of new drugs. This accounts for, for example, the influence of nicotine on cognition in Alzheimer's disease, which can be related both to a particular action on nicotinic receptors and to acting on brain networks in general [61].

Conclusion:

The development of new technology platforms can contribute to accelerate, diversify, and lower the cost of discovering and validating new nuclear imaging probes, biomarkers, radiotracers, and labeled drugs, as well as new radiotherapeutic agents. The wide implementation of nuclear imaging techniques for local use in research and clinical programs requires the invention of new, small and low-cost miniaturized particle-accelerators and generators for producing short-lived radioisotopes. The invention of new detector technologies for PET would contribute to enhance sensitivity as well as spatial and temporal resolution. In this paper we tried to take a brief about PET/MRI showing important sides considered in this technology.

Finally, the development of new iterative algorithms and high-speed/high-capacity computational systems for rapid image reconstruction; would allow image data to be converted to quantitative parametric images pertaining to biological and pharmacological processes in disease.

References

1- Giacomo Tondo, Marcello Esposito, George Dervenoulas, Heather Wilson, Marios Politis and Gennaro Pagano, Chapter 7 "Hybrid PET-MRI Applications in Movement Disorders" Volume 144, 2019, 211-257, (Link).
2- Zaidi, H., Diaz-Gomez, M., Boudraa, A., and Slosman, D. O. "Fuzzy clustering-based segmented attenuation correction in whole-body PET imaging. Physics in Medicine and Biology" 2002, 47(7), 1143–1160.
3- Martinez-Möller A, Eiber M, Nekolla SG, et al and J Nucl Med, "Workflow and scan protocol considerations for integrated whole-body PET/MRI in oncology", 2012, 53:1415–26.
4- Semelka RC, Kelekis NL, Thomasson D, Brown MA and Laub GA. HASTE "MR imaging: description of technique and preliminary results in the abdomen. J Magn Reson Imaging" 1996, 6:698–9
5- Dixon WT. "Simple proton spectroscopic imaging. Radiology" 1984, 153:189–94
6- Loening AM, Litwiller DV, Saranathan M and Vasanawala SS. "Increased speed and image quality for pelvic single-shot fast spin-echo imaging with variable refocusing flip angles and full- Fourier acquisition. Radiology" 2016, 282:561–8.
7- Bydder GM, Young IR and J Comput Assist Tomogr. "MR imaging: clinical use of the inversion recovery sequence", 1985, 9:659–75.
8- Pipe JG. "Motion correction with PROPELLER MRI: application to head motion and free- breathing cardiac imaging" Magn Reson Med. 1999, 42:963–9.
9- Pipe JG, Zwart N. "Turboprop: Improved PROPELLER imaging" Magn Reson Med. 2006, 55:380–5.
10- Hargreaves BA. "Rapid gradient-echo imaging. J Magn Reson Imaging" 2012, 36:1300–13.
11- Feng L, Axel L, Chandarana H, Block KT, Sodickson DK and Otazo R. "XD-GRASP: goldenangle radial MRI with reconstruction of extra motion state dimensions using compressed sensing" Magn Reson Med. 2015. (Link).
12- Lustig M, Donoho D, Pauly JM. "Sparse MRI: the application of compressed sensing for rapid MR imaging" Magn Reson Med. 2007, 58:1182–95.
13- Wollenweber SD, Ambwani S, Lonn AHR, et al. "Comparison of 4-class and continuous fat/water methods for whole-body, MR-based PET attenuation correction" IEEE Trans Nucl Sci. 2013, 60:3391–8.
14- Mehranian A, Zaidi H. "Impact of time-of-flight PET on quantification errors in MR imaging-based attenuation correction" J Nucl Med. 2015, 56:635–41.
15- Iagaru, Andrei & Hope, Thomas & Veit-Haibach, Patrick. "PET/MRI in oncology: Current clinical applications" 2018, (Link).
16- Du J, Bydder M, Takahashi AM, Chung CB. "Two-dimensional ultrashort echo time imaging using a spiral trajectory" Magn Reson Imaging. 2008, 26:304–12.
17- Yu J, Xue Y and Song HK. "Comparison of lung T2* during free-breathing at 1.5 T and 3.0 T with ultrashort echo time imaging" Magn Reson Med. 2011, 66:248–54.
18- Johnson KM, Fain SB, Schiebler ML and Nagle S. "Optimized 3D ultrashort echo time pulmonary MRI" Magn Reson Med. 2013, 70:1241–50.
19- Braun H, Ziegler S, Paulus DH and Quick HH. "Hybrid PET/MRI imaging with continuous table motion" Med Phys. 2012, 39:2735–45
20- Zaidi HI. "MR-guided attenuation correction a viable option for dual-modality PET/MR imaging?" Radiology. 2007, 244:639–42.
21- Martinez-Moeller A, Souvatzoglou M and Delso G. "Tissue classification as a potential approach for attenuation correction in whole-body PET/MRI: evaluation with PET/CT data" J Nucl Med. 2009, 50:520–6.

22- Eiber M, Martinez-Moeller A, Souvatzoglou M, et al. “Value of a Dixon-based MR/PET attenuation correction sequence for the localization and evaluation of PET-positive lesions” Eur J Nucl Med Mol Imaging. 2011, 38:1691–701.
23- Schulz V, Torres-Espallardo I, Renisch S, et al. “Automatic, three-segment, MRbased attenuation correction for whole-body PET/MR data” Eur J Nucl Med Mol Imaging. 2011, 38:138–52.
24- Catana C, van der Kouwe A, Benner T, et al. “Toward implementing an MRIbased PET attenuation-correction method for neurologic studies on the MR-PET brain prototype” J Nucl Med. 2010, 51:1431–8.
25- Hofmann M, Pichler B, Schöllkopf B, Beyer T. “Towards quantitative PET/MRI: a review of MR-based attenuation correction techniques” Eur J Nucl Med Mol Imaging. 2009, 36(suppl 1):S93–S104.
26- Ladefoged CN, Benoit D, Law I, Holm S, Kjær A, Højgaard L, Hansen AE and Andersen FL. “Region specific optimization of continuous linear attenuation coefficients based on UTE (RESOLUTE): application to PET/MR brain imaging” Phys Med Biol. 2015, 60(20):8047–65. (Link).
27- [4] Dominik Weishaupt, Victor D. Koechli and Borut Marincek, Chapter 3 “How does MRI work? An Introduction to the Physics and Function of Magnetic Resonance Imaging”, 1994, pp. 20-27.
28- [3] Vibhu Kapoor, Barry M. McCook, Frank S. Torok, “PET-CT Imaging”, 2004, pp. 531.
29- Ros Pablo, Delso Gaspar and Z. Sibylle, Chapter 1, “PETMRI Methodology and Clinical Applications”, 2014, pp. 15-18.
30- Vandenberghe S, Marsden PK. PET-MRI: a review of challenges and solutions in the development of integrated multimodality imaging. Phys Med Biol. 2015; 60(4):R115.
31- Visvikis D, Monnier F, Bert J, Hatt M, Fayad H. PET/MR attenuation correction: where have we come from and where are we going? Eur J Nucl Med. 2014; 41(6):1172–5.
32- eyer T, Lassen ML, Boellaard R, Delso G, Yaqub M, Sattler B, et al. Investigating the state-of-the-art in whole-body MR-based attenuation correction: an intra-individual, inter system, inventory study on three clinical PET/MR systems. MAGMA. 2016; 29(1):75–87. Epub 2016/01/08
33- Martinez-Moller A, Souvatzoglou M, Delso G, Bundschuh RA, Chefd’hotel C, Ziegler SI, et al. Tissue classification as a potential approach for attenuation correction in whole body PET/MRI: evaluation with PET/CT data. J Nucl Med. 2009; 50(4):520–526. Epub 2009/03/18.
34- Keereman V, Holen RV, Mollet P, Vandenberghe S. The effect of errors in segmented attenuation maps on PET quantification. Med Phys. 2011;38(11):6010–6019. 2011/11/04.
35- Dixon WT. Simple proton spectroscopic imaging, Radiology. 1984; 153(1):189–194, 1984/10/01.
36- Du J, Carl M, Bydder M, Takahashi A, Chung CB, Bydder GM. Qualitative and quantitative ultra short echo time (UTE) imaging of cortical bone. J Magn Reson. 2010:304–311, 2010/10/29.
37- Catana C, Van der Kouwe A, Benner T, Hamm C, Michel CJ, Fenchel M, et al. MR-based PET attenuation correction for neurological studies using dual-echo UTE sequences, 2010, p. 3953.
38- Wollenweber SD, Ambwani S, Lonn AHR, Mullick R, Wiesinger F, Piti Z, et al., editors. Evaluation of an atlas-based PET head attenuation correction using PET/CT & MR patient data. In: Nuclear Science Symposium and Medical Imaging Conference (NSS/MIC). IEEE; October 27 2012–November 3 2012.
39- Hofmann M, Steinke F, Scheel V, Charpiat G, Farquhar J, Aschoff P, et al. MRI-based attenuation correction for PET/MRI: a novel approach combining pattern recognition and atlas registration. J Nucl Med. 2008; 49(11):1875–1883. Epub 2008/10/18.
40- Khateri P, Saligheh Rad H, Jafari AH, Fathi Kazerooni A, Akbarzadeh A, Shojae Moghadam M, et al. Generation of a four-class attenuation map for MRI-based attenuation correction of PET data in the head area using a novel combination of STE/Dixon-MRI and FCM clustering. Mol Imaging Biol. 2015; 17(6):884–892. Epub 2015/04/29.
41- Paulus DH, Quick HH, Geppert C, Fenchel M, Zhan Y, Hermosillo G, et al. Whole-body

PET/MR imaging: quantitative evaluation of a novel model-based MR attenuation correction method including bone. J Nucl Med. 2015; 56(7):1061–6.
42- Delso G, Martinez-Moller A, Bundschuh RA, Nekolla SG, Ziegler SI. The effect of limited MR field of view in MR/PET attenuation correction. Med Phys. 2010; 37(6):2804–12. Epub 2010/07/17.
43- Mawlawi O, Erasmus JJ, Pan T, Cody DD, Campbell R, Lonn AH, et al. Truncation artifact on PET/CT: impact on measurements of activity concentration and assessment of a correction algorithm. AJR Am J Roentgenol. 2006; 186(5):1458–1467. Epub 2006/04/25.
44- Blumhagen JO, Ladebeck R, Fenchel M, Scheffler K. MR-based field-of-view extension in MR/PET: B0 homogenization using gradient enhancement (HUGE). Magn Reson Med, 2012.
45- Conti M. Why is TOF PET reconstruction a more robust method in the presence of inconsistent data? Phys Med Biol. 2011; 56(1):155–168. Epub 2010/12/02.
46- Kamel EM, Burger C, Buck A, von Schulthess GK, Goerres GW. Impact of metallic dental implants on CT-based attenuation correction in a combined PET/CT scanner. Eur Radiol. 2003; 13(4):724–728. Epub 2003/03/29.
47- Brendle C, Schmidt H, Oergel A, Bezrukov I, Mueller M, Schraml C, et al. Segmentation-based attenuation correction in positron emission tomography/magnetic resonance: erroneous tissue identification and its impact on positron emission tomography interpretation. Investing Radiol. 2015; 50(5):339–346. Epub 2015/01/15.
48- Davison H, Voert ET, Barbosa FDG, Veit-Haibach P, Delso G. Incorporation of TOF information reduces metal artifacts in simultaneous PET/MR: a simulation study. Investing Radiol 2015;50(7):423–9.
49- Schramm G, Maus J, Hofheinz F, Petr J, Lougovski A, Beuthien-Baumann B, et al. Evaluation and automatic correction of metal-implant-induced artifacts in MR-based attenuation correction in whole-body PET/MR imaging. Phys Med Biol. 2014; 59(11):2713–2726. Epub 2014/05/08.
50- Ladefoged C, Andersen F, Keller S, Löfgren J, Hansen A, Holm S, et al. PET/MR imaging of the pelvis in the presence of endoprostheses: reducing image artifacts and increasing accuracy through inpainting. Eur J Nucl Med. 2013:1–8.
51- Burger IA, Wurnig MC, Becker AS, Kenkel D, Delso G, Veit-Haibach P, et al. Hybrid PET/MR imaging: an algorithm to reduce metal artifacts from dental implants in Dixon-based attenuation map generation using a multiacquisition variable-resonance image combination sequence. J Nucl Med. 2015; 56(1):93–7.
52- Pan T, Mawlawi O, Nehmeh SA, Erdi YE, Luo D, Liu HH, et al. Attenuation correction of PET images with respiration-averaged CT images in PET/CT. J Nucl Med. 2005;46(9):1481–7. Epub 2005/09/15.
53- Delso G, Zeimpekis K, Wiesinger F, Khalighi M, Carl M, Veit-Haibach P. Impact of patient motion on bone attenuation maps. J Nucl Med. 2014; 55(supplement 1):2104.
54- Jensen RR, Olesen OV, Benjaminsen C, Højgaard L, Larsen R. Markerless PET motion correction: tracking in narrow gantries through optical fibers. IEEE nuclear science symposium and medical imaging conference (NSS/MIC); 2014.
55- -Lois C, Bezrukov I, Schmidt H, Schwenzer N, Werner M, Kupferschläger J, et al. Effect of MR contrast agents on quantitative accuracy of PET in combined whole-body PET/MR imaging. Eur J Nucl Med. 2012; 39(11):1756–66.
56- Ruhlmann V, Heusch P, Kuhl H, Beiderwellen K, Antoch G, Forsting M, et al. Potential influence of Gadolinium contrast on image segmentation in MR-based attenuation correction with Dixon sequences in whole-body 18F-FDG PET/MR. MAGMA. 2015. Epub 2015/12/17.
57- Tomohiro Kaneta, (2013, Feb 25). Guidelines for the Clinical Use of 18F-FDG-PET/MRI 2012[Online]. Available: http://jsnm.org/archives/2551/
58- Usman Bashir, Andrew Mallia, James Stirling, John Joemon, Jane MacKewn, Geoff Charles-Edwards, Vicky Goh and Gary J. Cook. (2015, September) "PET/MRI in Oncological Imaging: State of the Art." Diagnostics. Available: https://pdfs.semanticscholar.org/e79f/1f8587152b381137277de7d2fb7322f46706.pdf

59- Nainesh Parikh, Kent P. Friedman, Shetal N. Shah and Hersh Chandarana. (2016, February).” Practical guide for implementing hybrid PET/MR clinical service: lessons learned from our experience”. PMC. Available: https://www.ncbi.nlm.nih.gov/pmc/articles/PMC4534342/
60- H. Wehrl, A. Sauter, M. Judenhofer and B. Pichler, "Combined PET/MR Imaging — Technology and Applications", Technology in Cancer Research & Treatment, vol. 9, no. 1, 2010.
61- D. Bailey, G. Antoch, P. Bartenstein, H. Barthel, A. Beer, S. Bisdas, D. Bluemke, R. Boellaard, C. Claussen, C. Franzius, M. Hacker, H. Hricak, C. la Fougère, B. Gückel, S. Nekolla, B. Pichler, S. Purz, H. Quick, O. Sabri, B. Sattler, J. Schäfer, H. Schmidt, J. van den Hoff, S. Voss, W. Weber, H. Wehrl and T. Beyer, "Combined PET/MR: The Real Work Has Just Started. Summary Report of the Third International Workshop on PET/MR Imaging; February 17–21, 2014, Tübingen, Germany", Molecular Imaging and Biology, vol. 17, no. 3, 2015 [Online]. Available: https://www.ncbi.nlm.nih.gov/pmc/articles/PMC4422837/